

MHD flow and heat transfer in a nanofluid over a slender elastic sheet with variable thickness



K.V. Prasad ^{a,*}, K. Vajravelu ^b, Hanumesh Vaidya ^a, Robert A. Van Gorder ^c

^a Department of Mathematics, VSK University, Vinayaka Nagar, Ballari 583 105, Karnataka, India

^b Department of Mathematics, University of Central Florida, Orlando, FL 32816, USA

^c Mathematical Institute, University of Oxford, Andrew Wiles Building, Radcliffe Observatory Quarter, Woodstock Road, Oxford OX2 6GG, United Kingdom

ARTICLE INFO

Article history:

Received 28 December 2016

Received in revised form 11 March 2017

Accepted 20 March 2017

Available online 19 April 2017

Keywords:

Nanofluid flow

Heat transfer

Brownian diffusion

Thermophoresis

Transpiration

ABSTRACT

MHD flow and heat transfer characteristics in a nanofluid over a slender elastic sheet with variable thickness in the presence of variable fluid properties are analyzed. The nonlinear governing equations with suitable boundary conditions are initially cast into dimensionless form by similarity transformations and then the resulting equations are solved via the optimal homotopy analysis method (OHAM). The influences of the fluid viscosity, wall thickness, power index, Brownian motion, and thermophoresis parameters on flow, temperature, and nanoparticle volume fraction fields are analyzed graphically. The analysis reveals quite an interesting and substantial influence of transpiration (wall suction or injection) on the flow and heat transfer characteristics. The flow decelerated with suction and accelerated noticeably with increasing injection (blowing).

© 2017 Published by Elsevier B.V. This is an open access article under the CC BY-NC-ND license (<http://creativecommons.org/licenses/by-nc-nd/4.0/>).

Introduction

In recent years, nanofluids have attracted a great deal of attention due to their potential in enhancing the heat transfer. Nano-sized metallic particles, namely, aluminum, gold, copper, iron, or their oxides are used as colloidal agents with most common base fluids such as water, ethylene, glycol, toluene, or oil so that thermo-physical properties of heat transport of the base fluid can be improved. Choi [1] and Choi and Eastman [2] called the fluids laden with nanoparticles (1–100 nm) “nanofluids”. These nanofluids gained momentum and popularity due to their applications and paved the way to a new class of heat transfer fluids. Choi [1] proposed that the thermal conductivity of conventional liquids can be increased by adding nanoparticles to it. In continuation of [1], Choi and Eastman [2] established that the heat/thermal conductivity of any base fluid can be doubled by adding less than 1% of nanoparticles to it. Xuan et al. [3] simulated random motion and the aggregation process of the nanoparticles by applying Brownian motion theory and the model of diffusion-limited aggregation. Further, Buongiorno [4] concluded that the Brownian diffusion and the thermophoresis are the only important slip mechanisms, out of seven slip mechanisms, which can produce a relative velocity between the nanoparticles and the base fluid. Kuznetsov and Nield

[5] presented the results on the basis of [4] and proposed that the decreasing Nusselt number is a decreasing function of each of Nr , Nb and Nt . Kamyar et al. [6] employed a new Lattice-Boltzmann method (LBM) to analyze the fascinating behavior of cooling fluids containing ultrafine nanoparticles. Interestingly, most of these computational simulations are in concordance and agreement with the results from experiments. Rana and Bhargava [7] studied the nanofluid model which explains the effects of thermophoresis and Brownian motion on nanofluids. Rashidi et al. [8] extended the Rana and Bhargava [7] model to consider the effects of wall transpiration i.e. suction or injection. Recently, Anbuhezian et al. [9], Alsaedi et al. [10] and Mania and Bhargava [11] analyzed the effects of thermophoresis and Brownian motion on boundary layer flow of a nanofluid. Numerous studies have considered the nature of nanofluids which enhance the thermal conductivity and heat transfer characteristics through different geometries [12–20]. Readers can find a detailed review of nanofluids in the review article of Raja et al. [21].

All the above studies analyzed the characteristics of nanofluid flows by assuming constant thermophysical properties of the base fluid. However, it is evident from the works of Lai and Kulacki [22] that the physical properties of the ambient fluid may change with temperature, especially the fluid viscosity and the fluid thermal conductivity. For lubricating fluids, heat generated by internal friction and the corresponding rise in the temperature affects the physical properties of the nanofluid, and the properties of the fluid

* Corresponding author.

E-mail address: prasadkv2007@gmail.com (K.V. Prasad).

| | |
|---------------|---|
| a | constant in Eq. (2.5) |
| T | temperature (K) |
| T_r | constant in Eq. (2.5) |
| T_w | temperature of the plate (K) |
| T_∞ | ambient temperature (K) |
| ΔT | temperature difference (K) |
| D_T | thermophoretic diffusion coefficient (kg/ms K) |
| $D_{B\infty}$ | Brownian diffusion coefficient (kg/ms) |
| b | constant in Eq. (2.7) known as stretching rate $b > 0$ |
| B_0 | Uniform magnetic field (Tesla) |
| C_p | specific heat at constant pressure (J/kg K) |
| C_f | skin friction |
| f | dimensionless stream function |
| $K(T)$ | temperature dependent thermal conductivity (W/m K) |
| K_∞ | thermal conductivity of the fluid far away from the sheet (W/m K) |
| Le | lewis number |
| m | velocity exponent parameter |
| Mn | magnetic parameter |
| Nb | Brownian motion parameter |
| Nt | thermophoresis parameter |
| Nu_x | Nusselt number |
| Pr | Prandtl number |
| Re_x | local Reynolds number |
| Sh_x | Sherwood number |
| u, v | velocity components in the x and v directions (m/s) |

| | |
|----------|-----------------------|
| ∞ | condition at infinity |
| w | condition at the wall |

variable thickness; for details, see Fang et al. [27]). The variable thickness has applications to the vibration of orthotropic plates and is observed in many engineering applications more frequently than a flat surface such as machine design, architecture, nuclear reactor technology, naval structures, and acoustical components. Lee [28] studied the boundary layer flow over a slender body with variable thickness (the flow past a needle with variable diameters). Ishak et al. [29] examined the boundary layer flow over a horizontal thin needle and Ahmed et al. [30] analyzed mixed convection flow over a vertically moving thin needle. Recently, Khader and Megahed [31], Prasad et al. [32] analyzed the effects of various

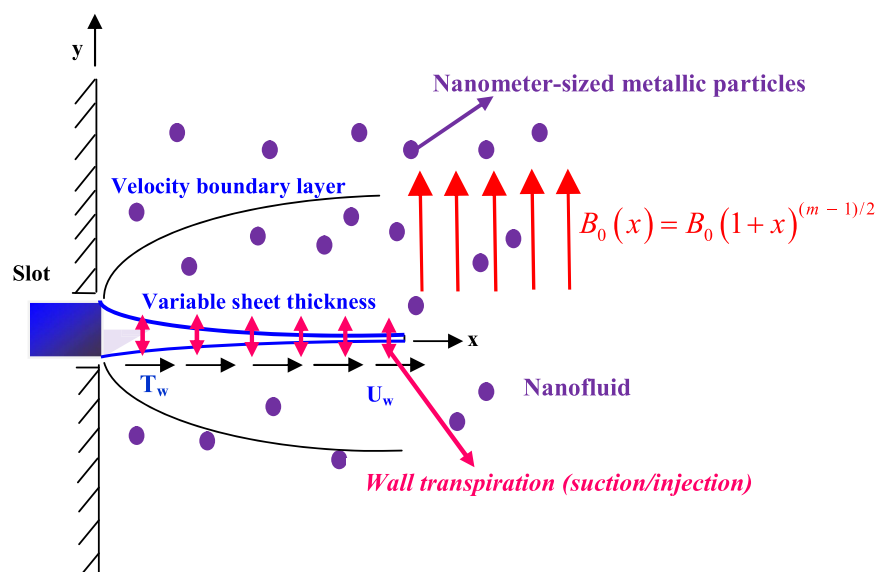


Fig. 1. Schematic diagram of the stretching sheet with variable thickness model.

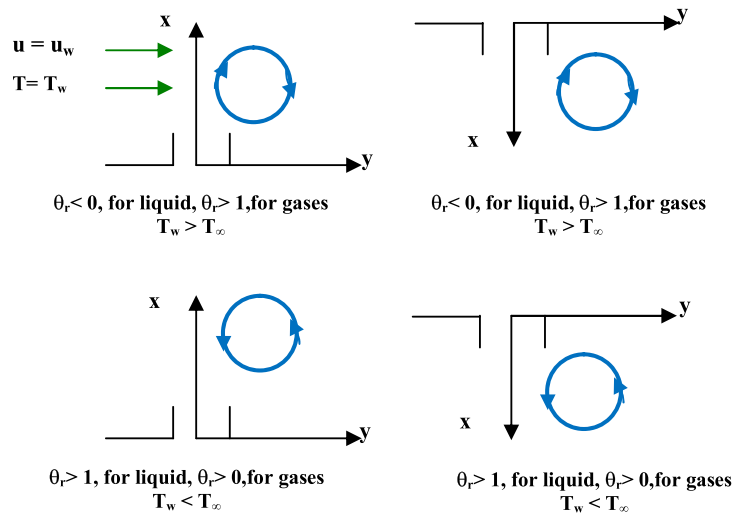


Fig. 2. Schematic diagram of an extrusion process and different physical situations.

physical parameters on the flow and heat transfer by considering this special form of stretching sheet.

In view of the above studies, in the present paper we analyze the effects of variable fluid properties on the nonlinear flow and heat transfer of a nanofluid in the presence of a transverse magnetic field with variable boundary-wall thickness. The governing nonlinear coupled system of ordinary differential equations for flow and heat transfer has been solved for various values of sundry parameters by the optimal homotopy analysis method (OHAM) [33,34]. The obtained results are analyzed for the nanofluid flow and heat transfer characteristics. The analysis reveals that the fluid flow is appreciably influenced by the physical parameters. It is expected that the results presented here will not only complement the existing literature but also provide useful information for industrial applications.

Mathematical formulation of the nanofluid model

Consider a steady two-dimensional boundary layer flow, heat and mass transfer of a viscous incompressible and electrically conducting nanofluid, in the presence of a transverse magnetic field $B(x)$, past an impermeable stretching sheet ($v_w = 0$, see Liao [35]) with variable thickness. The origin is located at the slit, through which the sheet is drawn in the fluid (see Figs. 1 and 2 for details). The x -axis is chosen in the direction of the motion and the y -axis is perpendicular to it. The stretching velocity of the surface is $U_w(x) = U_0(x+b)^m$ where U_0 is constant, b is the physical parameter related to stretching sheet, and m is the velocity exponent parameter with constant surface temperature T_w and the constant nanoparticle species diffusion C_w . The thermo-physical nanofluid properties are assumed to be isotropic and constant except for the fluid viscosity and the fluid thermal conductivity which are assumed to vary with temperature. We assume that the sheet is not flat but rather is defined as $y = A(x+b)^{(1-m)/2}$. The coefficient A is chosen as a small constant so that the sheet is sufficiently thin to avoid a measurable pressure gradient along the sheet ($\partial p/\partial x = 0$). For different applications, due to the acceleration or deceleration of the sheet, the thickness of the stretched sheet may decrease or increase with distance from the slot, which is dependent on the value of the velocity power index m . That is, in the case of $m > 0$, the thickness of the stretching sheet decreases, $m < 0$ increases thickness of the sheet, and $m = 1$ represents a

sheet of uniform thickness. For $m = 1$, the problem reduces to that of [23].

Under such assumptions, and by using the boundary layer approximation, the governing equations for mass, momentum, energy, and nanoparticle diffusion species for the nanofluid model in the presence of temperature dependent fluid properties are (see [7])

$$u \frac{\partial u}{\partial x} + v \frac{\partial v}{\partial y} = 0, \quad (2.1)$$

$$\rho_\infty \left(u \frac{\partial u}{\partial x} + v \frac{\partial u}{\partial y} \right) = \frac{\partial}{\partial y} \left(\mu \frac{\partial u}{\partial y} \right) - \sigma B_0^2(x)u, \quad (2.2)$$

$$u \frac{\partial T}{\partial x} + v \frac{\partial T}{\partial y} = \frac{1}{\rho_\infty C_p} \frac{\partial}{\partial y} \left(k(T) \frac{\partial T}{\partial y} \right) + \tau \left[D_B(C) \left(\frac{\partial C}{\partial y} \frac{\partial T}{\partial y} \right) + \frac{D_T}{T_\infty} \left(\frac{\partial T}{\partial y} \right)^2 \right], \quad (2.3)$$

$$u \frac{\partial C}{\partial x} + v \frac{\partial C}{\partial y} = \frac{\partial}{\partial y} \left(D_B(C) \frac{\partial C}{\partial y} \right) + \frac{D_T}{T_\infty} \frac{\partial^2 T}{\partial y^2}, \quad (2.4)$$

where u and v are the fluid velocity components measured along the x and y directions, respectively, ρ_∞ is the constant fluid density and μ is the coefficient of viscosity. Here in this paper μ is considered to vary as an inverse function of temperature (for details see Lai and Kulacki [22]) as

$$\mu = \frac{\mu_\infty}{[1 + \gamma(T - T_\infty)]} \quad \text{i.e.} \quad \frac{1}{\mu} = a(T - T_r) \quad (2.5)$$

where $a = \gamma/\mu_\infty$ and $T_r = T_\infty - 1/\gamma$. Here both a and T_r are constants and their values depend on the reference state and the small parameter γ reflecting a thermal property of the fluid. In general, $a > 0$ corresponds to liquid and $a < 0$ to gasses. T is the temperature; T_∞ and μ_∞ are the constant values of the temperature and coefficient of viscosity respectively away from the sheet. Also, σ is the electrical conductivity, $B_0^2(x) = B_0^2(x+b)^{m-1}$ is the magnetic field. This form of $B_0^2(x)$ has also been considered by several researchers to study MHD flow problems and to obtain similarity solution (see Prasad et al. [32] for details) over a moving or fixed flat plate. The parameter C_p is the specific heat at constant pressure and temperature dependent thermal conductivity. The species dependence on molecular diffusion of the diffusing species (diffusion

coefficient) in the fluid is assumed to vary as linear functions of temperature and concentration, respectively, in the forms

$$\frac{1}{\rho_{\infty} C_p} k(T) = \alpha_0 \left(\frac{k_{\infty}}{\rho_{\infty} C_p} \right) \left(1 + \varepsilon_1 \left(\frac{T - T_{\infty}}{T_w - T_{\infty}} \right) \right) \text{ and} \\ D_B(C) = D_{B\infty} \left(1 + \varepsilon_2 \left(\frac{C - C_{\infty}}{C_w - C_{\infty}} \right) \right), \quad (2.6)$$

where ε_1 and ε_2 are the small parameters, respectively, called variable thermal conductivity and the variable species diffusivity parameters. k_{∞} and $D_{B\infty}$ are the thermal conductivity and species diffusivity (Brownian diffusion coefficient) of the fluid far away from the sheet. Further, D_T is the thermophoretic diffusion coefficient, $\tau = (\rho_{\infty} c_p)_p / (\rho_{\infty} c_p)_f$ is the ratio between the effective heat capacity of the nanoparticle material and heat capacity of the fluid, ρ_{∞} is the density of the nanoparticle, c_{pf} is the specific heat of the fluid, and c_{pp} the specific heat of the nanoparticle (that is, $(\rho_{\infty} c_p)_p$ is the effective heat capacity of the nanoparticle material and $(\rho_{\infty} c_p)_f$ is the heat capacity of the fluid).

The boundary conditions for the physical problem under consideration are given by

$$u(x, y) = U_w = U_0(x + b)^m, \quad v(x, y) = 0, \quad T(x, y) = T_w, \\ C(x, y) = C_w, \quad \text{at } y = A(x + b)^{\frac{1-m}{2}}, \\ u(x, y) \rightarrow 0, \quad T(x, y) \rightarrow T_{\infty}, \quad C(x, y) \rightarrow C_{\infty} \text{ as } y \rightarrow \infty. \quad (2.7)$$

The positive and negative values of m represent two different cases, namely, stretching and shrinking sheets, respectively.

Similarity solutions for the nanofluid model

For the physical model considered in Mathematical formulation of the nanofluid model section, it is observed that the nanoparticle species diffusion, thermal, and momentum boundary layers exist when the surface temperature and the nanoparticle species diffusion differs from that of fluid temperature as well as nanoparticles species diffusion. Using the variable fluid properties (2.5), (2.6), the governing equations (2.2)–(2.4) in terms of stream function can be written as

$$\frac{\partial \psi}{\partial y} \frac{\partial^2 \psi}{\partial x \partial y} - \frac{\partial \psi}{\partial x} \frac{\partial^2 \psi}{\partial y^2} = \frac{1}{\rho_{\infty}} \left(\frac{\mu_{\infty}}{1 + \gamma(T - T_{\infty})} \frac{\partial^2 \psi}{\partial y^2} + \frac{\partial \psi}{\partial y} \frac{\partial}{\partial y} \left(\frac{\mu_{\infty}}{1 + \gamma(T - T_{\infty})} \right) \right) \\ - \frac{\sigma B_0^2(x)}{\rho_{\infty}} u, \quad (3.1)$$

$$\rho_{\infty} c_p \frac{\partial \psi}{\partial y} \frac{\partial T}{\partial x} - \left(\rho_{\infty} c_p \frac{\partial \psi}{\partial x} + \frac{k_{\infty} \varepsilon_1}{(T_w - T_{\infty})} \frac{\partial T}{\partial y} \right) \frac{\partial T}{\partial y} \\ = \left(k_{\infty} \left(1 + \varepsilon_1 \frac{T - T_{\infty}}{T_w - T_{\infty}} \right) \right) \frac{\partial^2 T}{\partial y^2} \\ + \tau \left[D_{B\infty} \left(1 + \varepsilon_2 \frac{C - C_{\infty}}{C_w - C_{\infty}} \right) \left(\frac{\partial C}{\partial y} \frac{\partial T}{\partial y} \right) + \frac{D_T}{T_{\infty}} \left(\frac{\partial T}{\partial y} \right)^2 \right], \quad (3.2)$$

$$\frac{\partial \psi}{\partial y} \frac{\partial C}{\partial x} - \left(\frac{\partial \psi}{\partial x} + \frac{D_{B\infty} \varepsilon_2}{(C_w - C_{\infty})} \frac{\partial C}{\partial y} \right) \frac{\partial C}{\partial y} = D_{B\infty} \left(1 + \varepsilon_2 \frac{C - C_{\infty}}{C_w - C_{\infty}} \right) \frac{\partial^2 C}{\partial y^2} + \frac{D_T}{T_{\infty}} \frac{\partial^2 T}{\partial y^2}. \quad (3.3)$$

The dimensionless stream function $\psi(x, y)$, is given by $(u, v) = \left(\frac{\partial \psi}{\partial y}, -\frac{\partial \psi}{\partial x} \right)$, which satisfies (2.1) automatically. We transform the system of Eqs. (3.1)–(3.3) into a dimensionless form. The suitable similarity transformations for the problem are

$$\psi(x, y) = f(\eta) \sqrt{\frac{2}{m+1}} U_0 v_{\infty} (x + b)^{\frac{m+1}{2}}, \quad \theta(\eta) = \frac{(T - T_{\infty})}{(T_w - T_{\infty})}, \\ \phi(\eta) = \frac{(C - C_{\infty})}{(C_w - C_{\infty})}, \quad \eta = y \sqrt{\frac{m+1}{2}} \frac{U_0}{v_{\infty}} (x + b)^{\frac{m-1}{2}}. \quad (3.4)$$

With Eq. (3.4), the velocity components can be written as

$$u = U_w f'(\eta) \text{ and } v = -\sqrt{\frac{m+1}{2}} U_0 (x + b)^{\frac{m-1}{2}} \left[f(\eta) + \eta f'(\eta) \left(\frac{m-1}{m+1} \right) \right]. \quad (3.5)$$

Here prime denotes differentiation with respect to η . In the present work, it is assumed $m > -1$ for the validity of the similarity variable. With the use of (3.4) and (3.5), Eqs. (3.1)–(3.3) and (2.7) reduces to

$$\left((1 - \theta/\theta_r)^{-1} \hat{f}'' \right)' + \hat{f} \hat{f}'' - 2m(1 + m)^{-1} \hat{f}^2 - Mn \hat{f}' = 0, \quad (3.6)$$

$$\left[(1 + \varepsilon_1 \hat{\theta}) \hat{\theta}' \right]' + \hat{\theta}' \left(Pr \hat{f} + Nb(1 + \varepsilon_2 \hat{\phi}) \hat{\phi}' + Nt \hat{\theta}' \right) = 0, \quad (3.7)$$

$$\left((1 + \varepsilon_2 \hat{\phi}) \hat{\phi}' + \frac{Nt}{Nb} \hat{\theta}' \right)' + Le \hat{f} \hat{\phi}' = 0, \quad (3.8)$$

and the corresponding boundary conditions are (for $m \neq -1$)

$$\hat{f}(\alpha) = \alpha \frac{1-m}{1+m}, \quad \hat{f}'(\alpha) = 1, \quad \hat{\theta}(\alpha) = 1, \quad \hat{\phi}(\alpha) = 1, \\ \hat{\theta}(\infty) = 0, \quad \hat{\phi}(\infty) = 0, \quad \hat{f}'(\infty) = 0. \quad (3.9)$$

The non-dimensional parameters θ_r , Mn , Pr , Nb , Nt , Le , and α , denoting fluid viscosity parameter, magnetic parameter, Prandtl number, Brownian motion parameter, thermophoresis parameter, the Lewis number, and wall thickness parameter, respectively, are given by

$$\theta_r = \frac{T_w - T_{\infty}}{T_w - T_{\infty}} = -\frac{1}{\gamma(T_w - T_{\infty})}, \quad Mn = \frac{2\sigma B_0^2}{\rho_{\infty} U_0 (1+m)}, \quad Pr = \frac{\nu_{\infty}}{\alpha_{\infty}}, \\ Nb = \frac{\tau D_{B\infty} (C_w - C_{\infty})}{\nu_{\infty}}, \quad Nt = \frac{\tau D_T (T_w - T_{\infty})}{T_{\infty} \nu_{\infty}}, \quad Le = \frac{\nu_{\infty}}{D_B}, \quad \alpha = A \sqrt{\frac{m+1}{2}} \frac{U_0}{v_{\infty}}. \quad (3.10)$$

The value of θ_r is determined by the viscosity of the fluid under consideration and the operating temperature difference. If θ_r is large, then $T_{\infty} - T_w$ is small and the effects of variable viscosity can be neglected. On other hand, for smaller values of θ_r , the fluid viscosity changes markedly with temperature. That is, the variable viscosity becomes very important. Here $\eta = \alpha$ indicates the plate surface. In order to facilitate the computation, we define $f(\xi) = \hat{f}(\eta)$, $\theta(\xi) = \hat{\theta}(\eta)$, and $\phi(\xi) = \hat{\phi}(\eta)$ where $\xi = \eta - \alpha$. Now the Eqs. (3.6)–(3.8) become

$$\left((1 - \theta/\theta_r)^{-1} f'' \right)' + f f'' - 2m(1 + m)^{-1} f'^2 - M n f' = 0, \quad (3.11)$$

$$[(1 + \varepsilon_1 \theta) \theta']' + \theta' (Pr f + Nb(1 + \varepsilon_2 \phi) \phi' + Nt \theta') = 0, \quad (3.12)$$

$$\left((1 + \varepsilon_2 \phi) \phi' + \frac{Nt}{Nb} \theta' \right)' + Le f \phi' = 0, \quad (3.13)$$

and the corresponding boundary conditions (2.17) for $m \neq -1$ are

$$f(0) = \alpha \frac{1-m}{1+m}, \quad f'(0) = 1, \quad \phi(0) = 1, \quad \theta(0) = 1, \\ = 1, \quad \lim_{\xi \rightarrow \infty} f'(\xi) = \lim_{\xi \rightarrow \infty} \theta(\xi) = \lim_{\xi \rightarrow \infty} \phi(\xi) = 0, \quad (3.14)$$

where the prime denotes the differentiation with respect to ξ . With reference to variable transformation, the integration domain will be fixed from 0 to ∞ . When we observe the boundary condition $f(0) = \alpha(1-m)/(1+m)$, it is clearly evident that transpiration (wall suction/ injection) can be observed for positive and negative values of m . In particular, $f(0) < 0$ (when $m > 1$) this has a similar effect to mass injection (blowing) at the wall. A large velocity index parameter leads to a large mass injection effect, which consequently increases skin friction and the wall shear stress. Further,

Table 1

Individual average residual error as a function of the number of iterations. CPU time required to calculate the solution is also listed. Parameter values are fixed at $Pr = 1.09$, $Le = 2.0$, $\varepsilon_1 = \varepsilon_2 = 0.1$, $\theta_r \rightarrow \infty$, $\alpha = 0.5$, $m = -0.33$, $Mn = 0$, $Nt = Nb = 0.5$. We have optimal convergence control parameter values of $h_f = -1.69980$, $h_\theta = -1.22605$, $h_\phi = -1.26912$.

| n | $\overline{\varepsilon_n^f}$ | $\overline{\varepsilon_n^\theta}$ | $\overline{\varepsilon_n^\phi}$ | CPU time (Sec) |
|-----|------------------------------|-----------------------------------|---------------------------------|----------------|
| 2 | 5.86×10^{-3} | 1.45×10^{-2} | 7.59×10^{-2} | 3.70 |
| 4 | 2.31×10^{-3} | 1.96×10^{-3} | 2.03×10^{-2} | 11.05 |
| 6 | 5.14×10^{-4} | 4.32×10^{-4} | 1.74×10^{-2} | 28.83 |
| 8 | 4.86×10^{-5} | 7.19×10^{-5} | 5.22×10^{-3} | 78.01 |
| 10 | 2.12×10^{-6} | 6.43×10^{-6} | 4.09×10^{-4} | 149.96 |
| 12 | 1.73×10^{-6} | 7.95×10^{-6} | 4.82×10^{-4} | 259.53 |
| 14 | 3.21×10^{-7} | 4.62×10^{-6} | 2.62×10^{-4} | 496.31 |
| 16 | 4.67×10^{-8} | 1.03×10^{-6} | 2.85×10^{-5} | 561.59 |
| 18 | 2.05×10^{-7} | 5.95×10^{-7} | 2.68×10^{-5} | 766.29 |
| 20 | 1.66×10^{-7} | 5.07×10^{-7} | 2.07×10^{-5} | 961.20 |

$f(0) > 0$ (when $m < 1$) is a case of suction and can significantly change the flow field. In addition to this, for $\alpha = 0$ or $m = 1$, the boundary condition reduces to $f(0) = 0$ which indicates an impermeable surface. For all practical purposes, the important physical quantities of interest are the local skin friction C_{f_x} , the local Nusselt number Nu_x , and the local Sherwood number Sh_x , defined as

$$\begin{aligned} C_{f_x} &= \frac{2 \nu_\infty (u_y)}{U_w^2} = \sqrt{2(m+1)} (\text{Re}_x)^{-1/2} f''(0), \\ Nu_x &= \frac{(x+b)(T_y)}{(T_w - T_\infty)} = -((m+1)\text{Re}_x/2)^{1/2} \theta'(0), \\ Sh_x &= \frac{(x+b)(C_y)}{(C_w - C_\infty)} = -((m+1)\text{Re}_x/2)^{1/2} \phi'(0), \end{aligned} \quad (3.15)$$

where $\text{Re}_x = U_w(x+b)/\nu_\infty$ is the local Reynolds number.

In the case of a flat plate ($m = 1$), the boundary layer flow and heat transfer problem degenerates. The solution for the velocity in the presence of a magnetic field turns out to be that found by Crane [23], and the solution for the temperature field can be written as a two parameter solution in terms of confluent hypergeometric series. In the absence of variable fluid properties, heat and mass transfer and magnetic field, solutions reduce to those of [27] for non-zero values of m .

Table 2

Comparison of results for $-f''(0)$ when $Mn = 0$, $\varepsilon_1 = \varepsilon_2 = Nt = Le = 0$, $Nb \rightarrow 0$ and $\theta_r \rightarrow \infty$.

| α | m | Fang et al. [27] By shooting method | Khader and Megahed [31] When $\lambda = 0$ By Chebyshev spectral method | Present work OHAM | | | |
|----------|------|--|---|----------------------|---------|--------------------------|-----------|
| | | | | $-f''(0)$ | $-h_f$ | \mathcal{E}_{10}^f | CPU Time |
| 0.5 | 10 | 1.0603 | 1.0603 | 1.0605077120653874 | 1.4149 | 3.28263×10^{-8} | 273.9668 |
| | 9 | 1.0589 | 1.0588 | 1.0511040757424492 | 1.4148 | 2.95971×10^{-8} | 269.7467 |
| | 7 | 1.0550 | 1.0551 | 1.0552402381500168 | 1.4141 | 2.18522×10^{-8} | 257.20091 |
| | 5 | 1.0486 | 1.0486 | 1.048791366557854 | 1.0145 | 1.24245×10^{-8} | 245.996 |
| | 3 | 1.0359 | 1.0358 | 1.035877993886442 | 1.0299 | 4.19553×10^{-9} | 245.527 |
| | 2 | 1.0234 | 1.0234 | 1.0230051676018523 | 1.4484 | 3.47652×10^{-9} | 267.506 |
| | 1 | 1.0 | 1.0 | 1.0 | 0 | 0 | 98.0504 |
| | 0.5 | 0.9799 | 0.9798 | 0.9791336007879321 | 1.1012 | 7.13672×10^{-8} | 264.260 |
| | 0 | 0.9576 | 0.9577 | 0.9571649276940054 | 1.6585 | 2.60785×10^{-6} | 230.339 |
| | -1/3 | 1.0000 | 1.0000 | 0.999835549839111 | 1.6689 | 1.95997×10^{-6} | 313.672 |
| | -1/2 | 1.1667 | 1.1666 | 1.1668932098461453 | 1.2991 | 2.04790×10^{-3} | 273.826 |
| | 10 | 1.1433 | 1.1433 | 1.1439820336033696 | 1.3572 | 2.97893×10^{-9} | 280.328 |
| | 9 | 1.1404 | 1.1404 | 1.1402440847765778 | 1.3584 | 2.77232×10^{-9} | 258.625 |
| | 7 | 1.1323 | 1.1323 | 1.1329048196291788 | 1.3624 | 2.33272×10^{-9} | 253.809 |
| 0.25 | 5 | 1.1186 | 1.1186 | 1.1181398433389969 | 1.3711 | 1.94457×10^{-9} | 304.807 |
| | 3 | 1.0905 | 1.0904 | 1.090832184327589 | 0.9463 | 1.8803×10^{-9} | 278.567 |
| | 1 | 1.0 | 1.0 | 1.0 | 0 | 0 | 101.036 |
| | 0.5 | 0.9338 | 0.9337 | 0.9330216794465643 | 1.50028 | 2.09957×10^{-8} | 252.132 |
| | 0 | 0.7843 | 0.7843 | 0.7840615830209784 | 1.2391 | 1.02799×10^{-6} | 238.463 |
| | -1/3 | 0.5000 | 0.5000 | 0.49999454048648743 | 0.8643 | 1.94672×10^{-5} | 241.383 |
| | -1/2 | 0.0833 | 0.08322 | 0.08330568175024846 | 1.3937 | 5.33716×10^{-5} | 265.181 |

Semi-Analytical numerical solution method

The governing equations are highly nonlinear, coupled ODEs with variable coefficients. We use the optimal homotopy analysis method (OHAM) to obtain appropriate analytic solutions to Eqs. (3.11)–(3.13) with associated boundary conditions (3.14). The OHAM is based on the homotopy concept from topology. In this regard, a nonlinear problem is transformed into an infinite number of linear sub-problems. In the frame of OHAM, we have great freedom to choose the auxiliary linear operators and initial approximations. This is advantageous over other iterative techniques where convergence is largely tied to a good initial approximation of the solution. The OHAM differs from other analytic approximation methods as it does not depend on small or large physical parameters. This is achieved by inclusion of an artificial “convergence control parameter,” which guarantees convergence of the solution series. The OHAM has been successfully applied to a wide variety of nonlinear problems (see [33,34]).

We choose the auxiliary linear operators as

$$\mathcal{L}_f = \frac{d^3}{d\xi^3} - \frac{d}{d\xi}, \quad \mathcal{L}_\theta = \frac{d^2}{d\xi^2} - f, \quad \text{and} \quad \mathcal{L}_\phi = \frac{d^2}{d\xi^2} - f. \quad (4.1)$$

Initial approximations satisfying the boundary conditions (3.14) are found to be

$$f_0(\xi) = 1 + \alpha \left(\frac{1-m}{1+m} \right) - e^{-\xi}, \quad \theta_0(\xi) = e^{-\xi}, \quad \text{and} \quad \phi_0(\xi) = e^{-\xi}.$$

Let us consider the so-called zero-th order deformation equations

$$(1-q)\mathcal{L}_f[\hat{f}(\xi; q) - f_0(\xi)] = qH_f(\xi)h_fN_f[\hat{f}(\xi; q), \hat{\theta}(\xi; q)], \quad (4.2)$$

$$(1-q)\mathcal{L}_\theta[\hat{\theta}(\xi; q) - \theta_0(\xi)] = qH_\theta(\xi)h_\theta N_\theta[\hat{\theta}(\xi; q), \hat{f}(\xi; q), \hat{\phi}(\xi; q)], \quad (4.3)$$

$$(1-q)\mathcal{L}_\phi[\hat{\phi}(\xi; q) - \phi_0(\xi)] = qH_\phi(\xi)h_\phi N_\phi[\hat{\phi}(\xi; q), \hat{\theta}(\xi; q), \hat{f}(\xi; q)]. \quad (4.4)$$

K.V. Prasad et al./Results in Physics 7 (2017) 1462–1474

1467

Here $q \in [0, 1]$ is an embedding parameter, while $h_f \neq 0$, $h_\theta \neq 0$ and $h_\phi \neq 0$ are the convergence control parameters, and the nonlinear differential operators are defined from Eqs. (3.11)–(3.13) as

$$\mathcal{N}_f[\hat{f}, \hat{\theta}] = \left(1 - \frac{\theta}{\theta_r}\right) \frac{\partial^3 \hat{f}}{\partial \xi^3} + \left(\frac{1}{\theta_r}\right) \frac{\partial^2 \hat{f}}{\partial \xi^2} \frac{\partial \hat{\theta}}{\partial \xi} + \left(1 - \frac{\theta}{\theta_r}\right)^2 \hat{f} \frac{\partial^2 \hat{f}}{\partial \xi^2} - \left(\frac{2m}{m+1}\right) \left(1 - \frac{\theta}{\theta_r}\right)^2 \left(\frac{\partial \hat{f}}{\partial \xi}\right)^2 - Mn \left(1 - \frac{\theta}{\theta_r}\right)^2 \frac{\partial \hat{f}}{\partial \xi}, \quad (4.5)$$

$$\mathcal{N}_\theta[\hat{f}, \hat{\theta}, \hat{\phi}] = \frac{\partial^2 \hat{\theta}}{\partial \xi^2} + \varepsilon_1 \hat{\theta} \frac{\partial^2 \hat{\theta}}{\partial \xi^2} + \varepsilon_1 \left(\frac{\partial \hat{\theta}}{\partial \xi}\right)^2 + Pr \hat{f} \frac{\partial \hat{\theta}}{\partial \xi} + Nb \frac{\partial \hat{\theta}}{\partial \xi} \frac{\partial \hat{\phi}}{\partial \xi} + \varepsilon_2 \frac{\partial \hat{\theta}}{\partial \xi} \hat{\phi} \frac{\partial \hat{\phi}}{\partial \xi} + Nt \left(\frac{\partial \hat{\theta}}{\partial \xi}\right)^2, \quad (4.6)$$

$$\mathcal{N}_\phi[\hat{f}, \hat{\theta}, \hat{\phi}] = \frac{\partial^2 \hat{\phi}}{\partial \xi^2} + \varepsilon_2 \hat{\phi} \frac{\partial^2 \hat{\phi}}{\partial \xi^2} + \varepsilon_2 \left(\frac{\partial \hat{\phi}}{\partial \xi}\right)^2 + \left(\frac{Nt}{Nb}\right) \frac{\partial^2 \hat{\phi}}{\partial \xi^2} + Le \hat{f} \frac{\partial \hat{\phi}}{\partial \xi}. \quad (4.7)$$

We choose the auxiliary functions as $H_f(\xi) = H_\theta(\xi) = H_\phi(\xi) = e^{-\xi}$. It can be seen from Eqs. (4.2)–(4.4) that when $q = 0$, we have $\hat{f}(\xi; 0) = f_0(\xi)$, etc., while when $q = 1$, we have $\hat{f}(\xi; 1) = f(\xi)$, etc., so we recover the exact solutions when $q = 1$. Expanding in q , we write $\hat{f}(\xi; q) = f_0(\xi) + \sum_{n=1}^{\infty} f_n(\xi) q^n$, $\hat{\theta}(\xi; q) = \theta_0(\xi) + \sum_{n=1}^{\infty} \theta_n(\xi) q^n$ and $\hat{\phi}(\xi; q) = \phi_0(\xi) + \sum_{n=1}^{\infty} \phi_n(\xi) q^n$. As q varies from 0 to 1, the homotopy solutions vary from the initial approximations to the solutions of interest. It should be noted that the homotopy solutions contain the unknown convergence control parameters $h_f \neq 0$, $h_\theta \neq 0$, and $h_\phi \neq 0$, which can be used to adjust and control

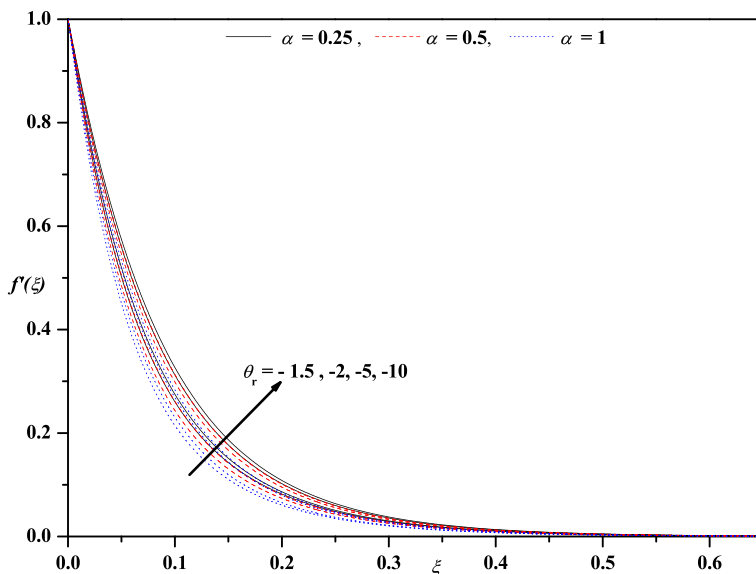


Fig. 3a. Horizontal velocity profiles for different values of α and θ_r with $m = 0.5$, $Pr = 1.09$, $Le = 1.5$, $\varepsilon_1 = \varepsilon_2 = 0.1$, $Nb = Nt = 0.5$, $Mn = 0.2$.

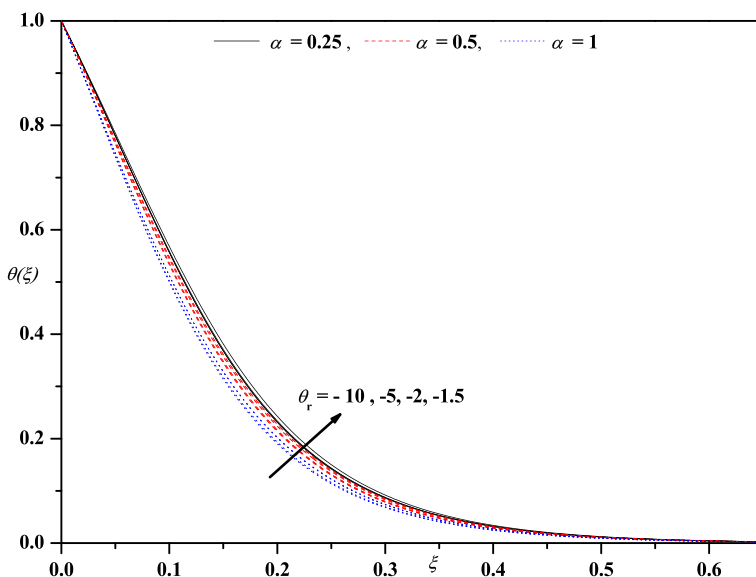


Fig. 3b. Temperature profiles for different values of α and θ_r with $m = 0.5$, $Pr = 1.09$, $Le = 1.5$, $\varepsilon_1 = \varepsilon_2 = 0.1$, $Nb = Nt = 0.5$, $Mn = 0.2$.

the convergence region and the rate of convergence of the series solution. To obtain the approximate solutions, we recursively solve the so-called n th-order deformation equations

$$\begin{aligned}\mathcal{L}_f[f_n(\xi) - \chi_n f_{n-1}(\xi)] &= h_f \mathcal{R}_n^f, & \mathcal{L}_\theta[\theta_n(\xi) - \chi_n \theta_{n-1}(\xi)] \\ &= h_\theta \mathcal{R}_n^\theta, & \mathcal{L}_\phi[\phi_n(\xi) - \chi_n \phi_{n-1}(\xi)] = h_\phi \mathcal{R}_n^\phi,\end{aligned}$$

$$\mathcal{R}_n^f = \frac{1}{(n-1)!} \left. \frac{\partial^{n-1} \mathcal{N}_f[\hat{f}(\xi; q), \hat{\theta}(\xi; q)]}{\partial q^{n-1}} \right|_{q=0},$$

$$\mathcal{R}_n^\theta = \frac{1}{(n-1)!} \left. \frac{\partial^{n-1} \mathcal{N}_\theta[\hat{f}(\xi; q), \hat{\theta}(\xi; q)]}{\partial q^{n-1}} \right|_{q=0},$$

$$\mathcal{R}_n^\phi = \frac{1}{(n-1)!} \left. \frac{\partial^{n-1} \mathcal{N}_\phi[\hat{f}(\xi; q), \hat{\theta}(\xi; q)]}{\partial q^{n-1}} \right|_{q=0}, \quad \chi_n = \begin{cases} 0, & n \leq 1, \\ 1, & n > 1. \end{cases}$$

In practice, we can only calculate finitely many terms in the homotopy series solution. We therefore define the k th order approximate solution can by the partial sums

$$f_{[k]}(\xi) = f_0(\xi) + \sum_{n=1}^k f_n(\xi), \quad \theta_{[k]}(\xi) = \theta_0(\xi) + \sum_{n=1}^k \theta_n(\xi) \text{ and}$$

$$\phi_{[k]}(\xi) = \phi_0(\xi) + \sum_{n=1}^k \phi_n(\xi).$$

With these approximations, we may evaluate the residual error and minimize it over the parameters h_f , h_θ and h_ϕ in order to obtain the optimal value of h_f , h_θ and h_ϕ giving the least possible residual error. To do so, one may use the integral of squared residual errors, however this is very computationally demanding. To get around this, we use the averaged squared residual errors, defined by

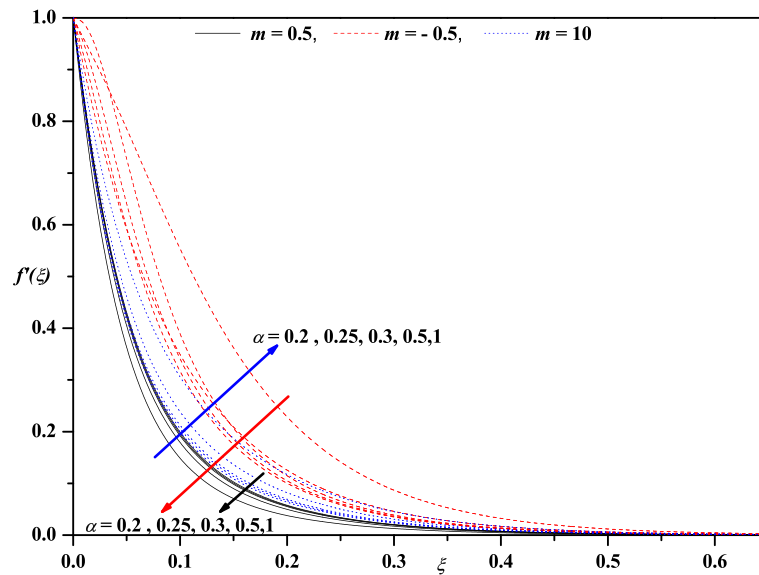


Fig. 4a. Horizontal velocity profiles for different values of m and α with $\theta_r = 1.5$, $Pr = 1.09$, $Le = 1.5$, $\varepsilon_1 = \varepsilon_2 = 0.1$, $Nb = Nt = 0.5$, $Mn = 0.2$.

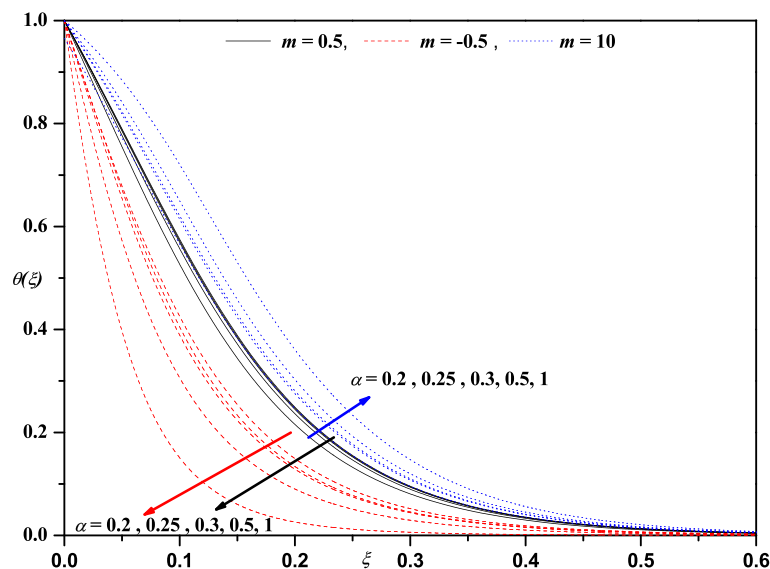


Fig. 4b. Temperature profiles for different values of m and α with $Mn = 0.2$, $\theta_r = 1.5$, $Pr = 1.09$, $Le = 1.5$, $\varepsilon_1 = \varepsilon_2 = 0.1$, $Nb = Nt = 0.5$.

$$\overline{\mathcal{E}}_n^f(h_f) = \frac{1}{M+1} \sum_{k=0}^M (\mathcal{N}_f[f_{[M]}(\xi_k), \theta_{[M]}(\xi_k)])^2,$$

$$\overline{\mathcal{E}}_n^\theta(h_\theta) = \frac{1}{M+1} \sum_{k=0}^M (\mathcal{N}_\theta[f_{[M]}(\xi_k), \theta_{[M]}(\xi_k), \phi_{[M]}(\xi_k)])^2,$$

$$\overline{\mathcal{E}}_n^\phi(h_\phi) = \frac{1}{M+1} \sum_{k=0}^M (\mathcal{N}_\phi[f_{[M]}(\xi_k), \theta_{[M]}(\xi_k), \phi_{[M]}(\xi_k)])^2,$$

where $\xi_k = k/M$, $k = 0, 1, 2, \dots, M$. For different order approximations, the CPU time required for obtaining the approximate solutions will vary. Table 1 lists the values of individual average residual errors by considering the optimal values of $h_f = -1.69980$, $h_\theta = -1.22605$, $h_\phi = -1.26912$, which have been obtained by minimizing the averaged residual errors at the 10th order approximation. As the number of terms in the approximation is increased, Table 1 shows that the CPU time required increases, while the averaged squared residual error decreases continuously. As such, by taking the order of approximation large enough, and by selecting the convergence control parameters to minimize the averaged squared residual error, we can obtain reasonably accurate approximate solutions.

Results and discussion

The system of ordinary differential equations (3.11)–(3.13) is one which is highly non-linear and coupled. Exact analytical solutions for the complete set of equations subject to the boundary conditions (3.14) are not possible. The system of equations is solved analytically via efficient OHAM. It can be shown that, when nanofluid effects and thermos-physical fluid properties are removed, the present results agree very well with those of [27,31] (See Table 2). It is essential to note that, θ_r is negative for liquids and positive for gasses. This is due to the fact that viscosity of a liquid decreases with increasing temperature while it increases for gasses. Hence, we have considered negative values of θ_r . The computed numerical values for $f''(0)$, $\theta'(0)$, and $\phi'(0)$ are tabulated in Table 3.

Fig. 3 illustrates the effect of different values of θ_r and α on $f'(\xi)$ and $\theta(\xi)$, respectively. It is noticed that $f'(\xi)$ decreases for increas-

ing values of θ_r . Further, as $\theta_r \rightarrow 0$, the boundary layer thickness decreases and the velocity distribution asymptotically tends to zero. This may be attributed to the fact that, for a given fluid (air or water), when γ is fixed, lesser θ_r implies higher temperature difference between the wall and the ambient fluid. Hence the results show that θ_r has a substantial effect on $f'(\xi)$ and hence on $f''(0)$. A similar trend can be observed for increasing values of α whereas in the case of $\theta(\xi)$, the effect of θ_r is quite opposite. Fig. 4 depicts the effect of α and m on $f'(\xi)$, $\theta(\xi)$, and $\phi(\xi)$. When $m > 1$, all the three profiles increase for increasing values of α , and the reverse trend may be seen in the case of $m < 1$. This can be explained with the help of the boundary condition $f(0) = \alpha(1-m)/(1+m)$, since transpiration (suction and blowing) can be noticed for different values of m . In particular, when $m > 1$ ($f(0) < 0$), this has a similar effect to mass injection at the wall, while $-1 < m < 1$ ($f(0) > 0$) is a case of suction which can significantly change the flow field. The flow is observed to be strongly decelerated with suction whereas it is accelerated noticeably with increasing injection (blowing). The suction causes the boundary layer to stick more closely to the wall which leads to a drop in velocity. Momentum boundary layer thickness is therefore decreased with suction. Conversely, injection adds nanofluid mass via lateral mass flux through the sheet and this assists momentum development, enhancing velocity and causing a concomitant increase in momentum boundary layer thickness. In the case of suction ($1 > m > -1, f(0) > 0$), temperature and concentration are found to be strongly decreased. Injection enhances both temperature and nanoparticle concentration. Thermal and concentration boundary layer thickness for the injection case are significantly greater than for the suction case. Effectively suction achieves a strong suppression of nano-particle species diffusion and also regulates the diffusion of thermal energy (heat) in the boundary layer. This response to suction has significant effects on the constitution of engineered nanofluids and shows that suction is an excellent mechanism for achieving flow control, cooling, and nano-particle distribution in nanofluid fabrication. The effect of m on $f'(\xi)$, $\theta(\xi)$, and $\phi(\xi)$ is demonstrated in Fig. 5. We observe that velocity profiles decrease initially with increasing m near the surface to a certain point within the boundary layer, but will increase beyond a certain distance η before decaying to zero. It is interesting to note that, at a particular point, change in m is insignificant within the boundary layer. Physically, a change in

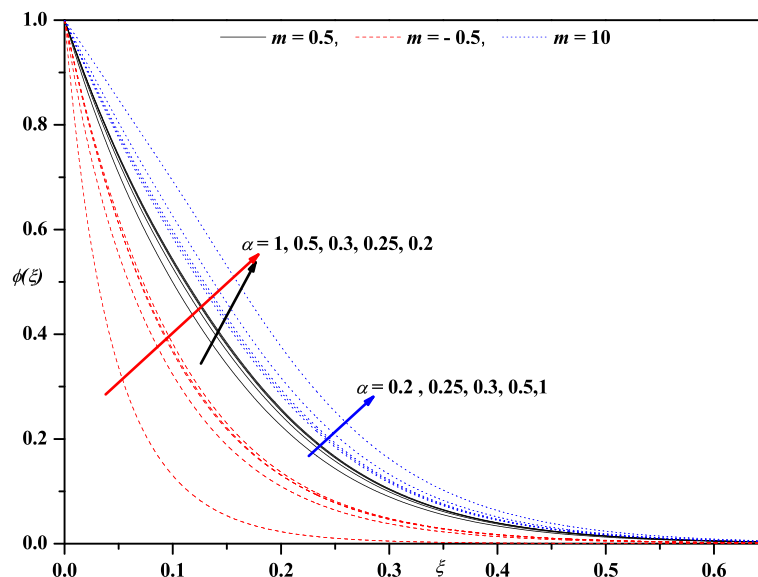


Fig. 4c. Concentration profiles for different values of m and α with $Mn = 0.2$, $\theta_r = 1.5$, $Pr = 1.09$, $Le = 1.5$, $\varepsilon_1 = \varepsilon_2 = 0.1$, $Nt = Nb = 0.5$.

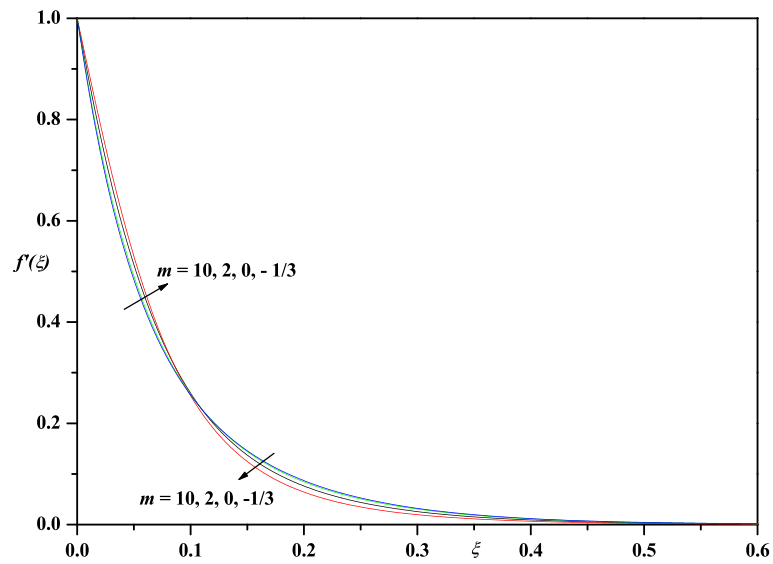


Fig. 5a. Velocity profiles for different values of m with $\alpha = 0.25$, $Pr = 1.09$, $Le = 1.5$, $\theta_r = -1.5$, $\varepsilon_1 = \varepsilon_2 = 0.1$, $Nb = Nt = 0.5$, $Mn = 0.2$.

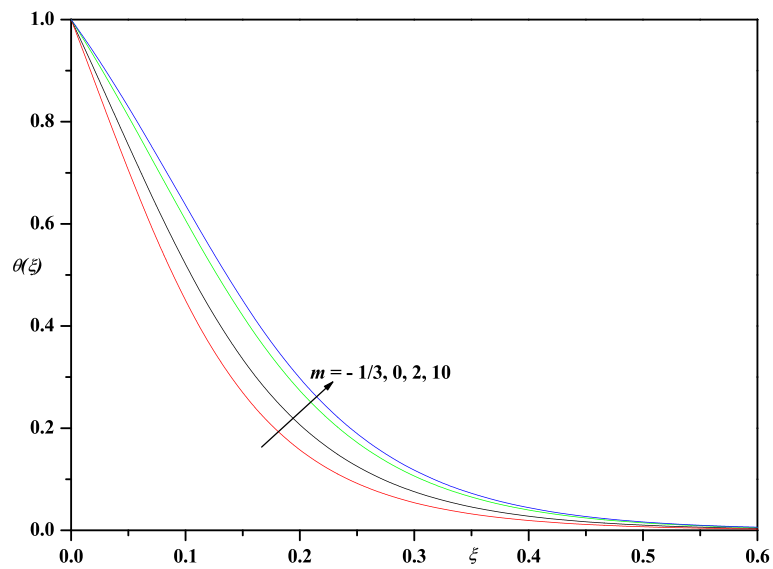


Fig. 5b. Temperature profiles for different values of m with $\alpha = 0.25$, $Pr = 1.09$, $Le = 1.5$, $\theta_r = -1.5$, $\varepsilon_1 = \varepsilon_2 = 0.1$, $Nb = Nt = 0.5$, $Mn = 0.2$.

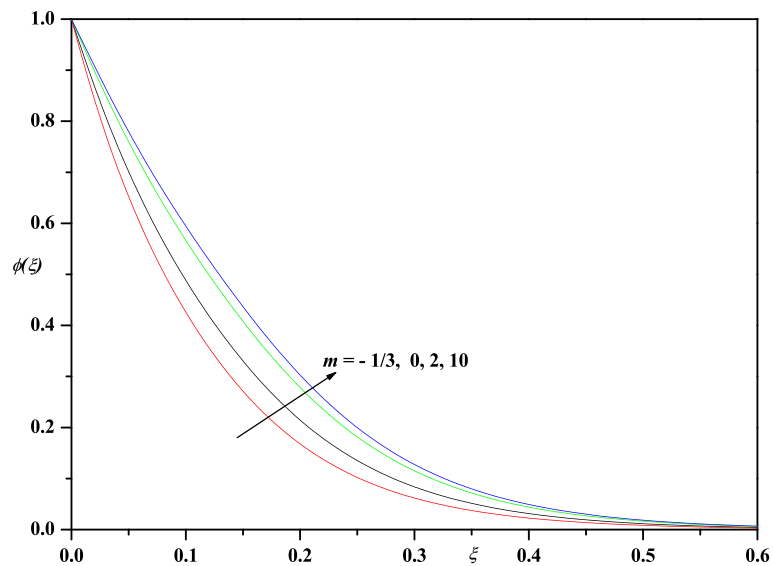


Fig. 5c. Concentration profiles for different values of m with $\alpha = 0.25$, $Pr = 1.09$, $Le = 1.5$, $\theta_r = -1.5$, $\varepsilon_1 = \varepsilon_2 = 0.1$, $Nb = Nt = 0.5$, $Mn = 0.2$.

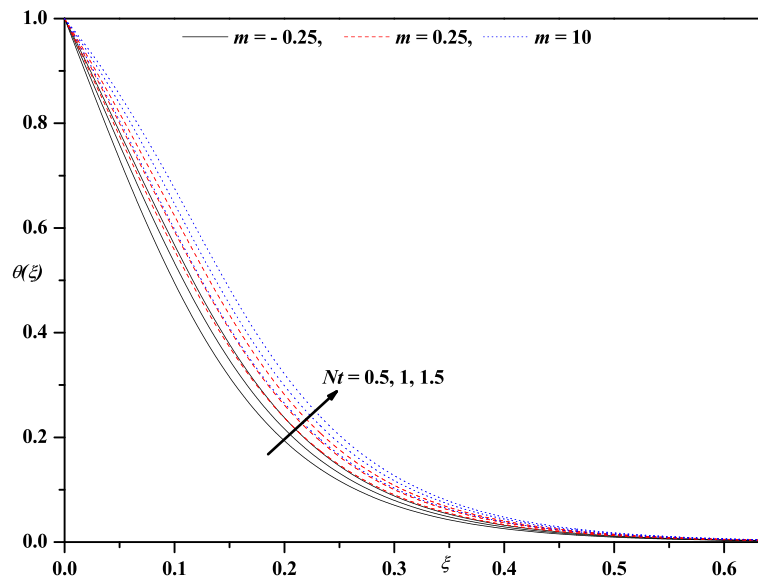


Fig. 6a. Temperature profiles for different values of m and Nt with $Nb = 0.5$, $\theta_r = 1.5$, $Pr = 1.09$, $Le = 1.5$, $\varepsilon_1 = \varepsilon_2 = 0.1$, $\alpha = 0.25$, $Mn = 0.2$.

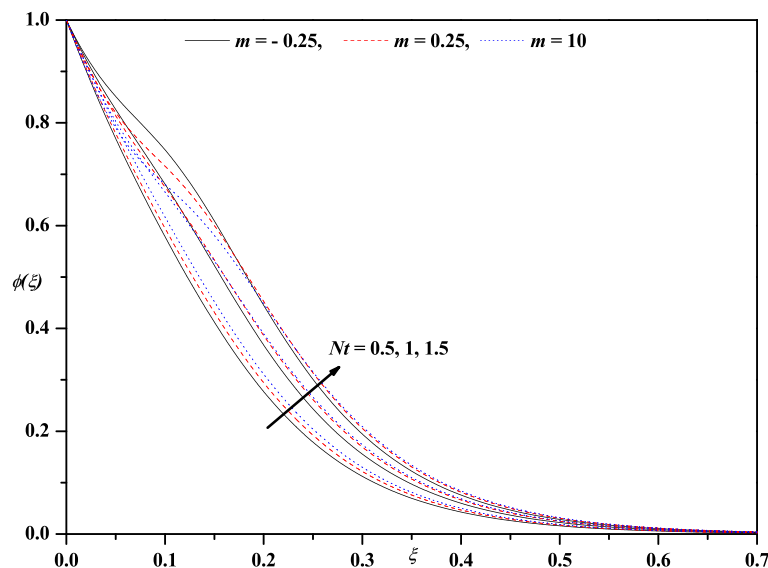


Fig. 6b. Concentration profiles for different values of m and Nt with $Nb = 0.5$, $\theta_r = 1.5$, $Pr = 1.09$, $Le = 1.5$, $\varepsilon_1 = \varepsilon_2 = 0.1$, $\alpha = 0.25$, $Mn = 0.2$.

the values of m means stretching the sheet linearly, quadratically, cubically, etc.; $m > 1$ indicates a decrease in the thickness of the surface and $m < 1$ indicates the increase the thickness of the surface; whereas $m = 1$ is the flat surface case. We observe that $\theta(\xi)$ and $\phi(\xi)$ increase uniformly with m .

Fig. 6 shows the influence of Nt on $\theta(\xi)$ and $\phi(\xi)$. Increasing thermophoresis assists both thermal and species diffusion by enhancing the boundary layer thickness. An increase in Nt (increase in thermophoresis force) tends to move particles from hot to cold regions, thereby increasing the nanoparticles volume fraction and enhancing nanoparticle concentration boundary layer thickness. Fig. 7 demonstrates that an increase in Nb (smaller nano-particles) elevates the temperature profiles and enhances the thermal conduction. Moreover, larger values of Nb will stifle

the diffusion of nanoparticles away from the surface, which results in a decrease in nano-particle concentration values in the boundary layer.

The impact of the physical parameters on $f''(0)$, $\theta'(0)$, and $\phi'(0)$ is presented in Table 3. We notice a decrease in the skin friction as Mn increases, while the opposite behavior is observed for the local Nusselt number and the local Sherwood number. This clearly manifests that the transverse magnetic field opposes the transport phenomena. The variation in Lorentz force may be attributed to the variation of Mn . The Lorentz force produces resistance to the transport phenomena and hence skin friction. Furthermore, an increase in both ε_1 or ε_2 results in an increase in each of the skin friction, local Nusselt number, and the local Sherwood number.

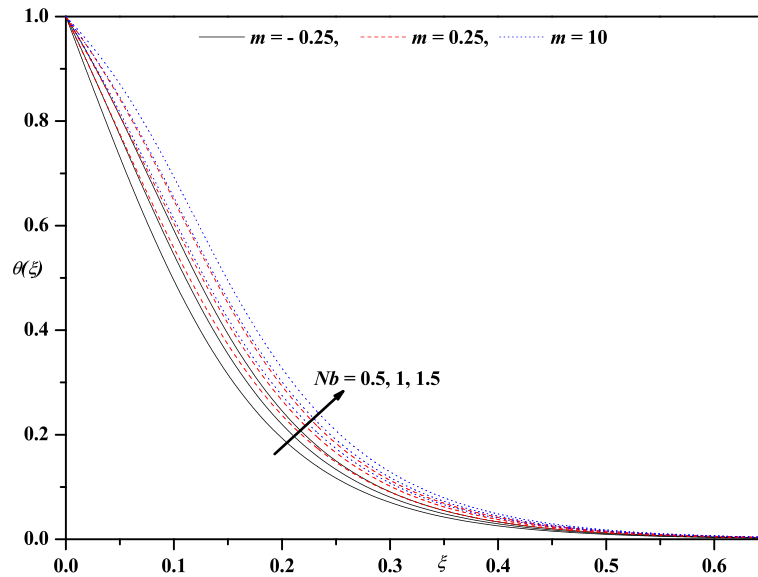


Fig. 7a. Temperature profiles for different values of m and Nb with $Nt = 0.5$, $\theta_r = 1.5$, $Pr = 1.09$, $Le = 1.5$, $\varepsilon_1 = \varepsilon_2 = 0.1$, $\alpha = 0.25$, $Mn = 0.2$.

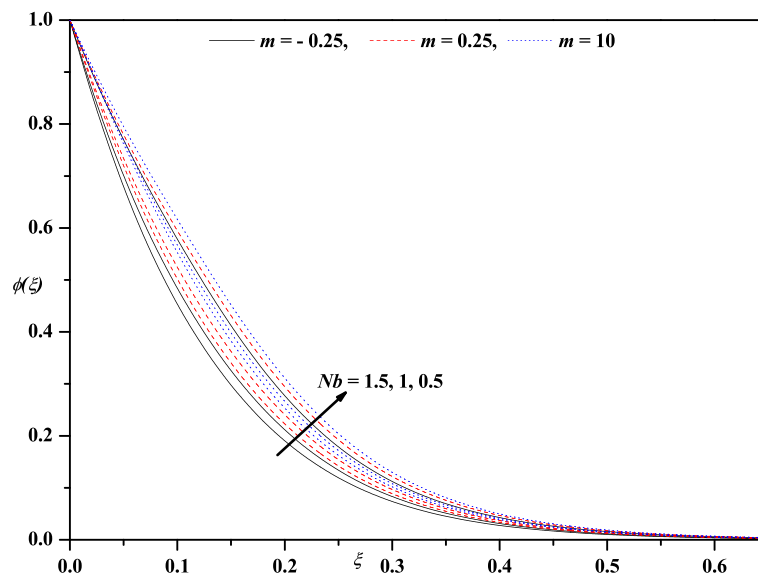


Fig. 7b. Concentration profiles for different values of m and Nb with $Nt = 0.5$, $\theta_r = 1.5$, $Pr = 1.09$, $Le = 1.5$, $\varepsilon_1 = \varepsilon_2 = 0.1$, $\alpha = 0.25$, $Mn = 0.2$.

Conclusions

Some of the interesting conclusions are as follows:

- An increase in the wall thickness parameter results in increase and decrease of the velocity, temperature, and concentration fields according as $m > 1$ or $1 > m > -1$.
- Increasing the power index parameter exhibits the decrease and increase of the velocity within the boundary layer near the surface.
- The nonlinear nature of the stretching surface has a significant impact on the boundary layer. The effect of transpiration (suction and blowing) can be noticed for different values of power index parameter. The flow decelerated with suction and accelerated noticeably with increasing injection (blowing).
- An increase in the temperature is due to an increase either in Brownian motion parameter or in the thermophoresis parameter.

- The temperature of the fluid increases and the nanoparticle volume fraction decreases with an increase in the Brownian motion parameter.
- An increase in the thermal, as well as nanoparticle concentration profiles, is due to the increase in the thermophoresis parameter; but in the case of the Brownian motion parameter, temperature profiles increase and concentration profiles decrease.
- An increase in the Nusselt number and the Sherwood number is due to the increase in the variable thermal conductivity, but in the case of variable species diffusivity parameter, the Nusselt number increases and Sherwood number decreases.

Acknowledgements

The authors thank Professor Michael Taylor for reading and editing the manuscript and also authors appreciate the construc-

tive comments of the reviewer which led to definite improvement in the paper.

References

- [1] Choi S. Enhancing thermal conductivity of fluids with nanoparticle. In: Siginer DA, Wang HP, editors. Developments and applications of non-Newtonian flows, 66. ASME; 1995. p. 99–105. MD 231 and FED.
- [2] Choi SUS, Eastman JA. Enhancing thermal conductivities of fluids with nanoparticles. In: Int. mech. engg. congress and exposition. San Francisco, USA: ASME; 1995.
- [3] Xuan Y, Li Q, Hu W. Aggregated structure and thermal conductivity of nanofluids. *AIChE J* 2003;49:1038–43.
- [4] Buongiorno J. Convective transport in nano fluids. *J Heat Mass Transfer ASME* 2006;128:240–50.
- [5] Kuznetsov AV, Nield DA. Natural convective boundary-layer flow of a nanofluid past a vertical plate. *Int J Therm Sci* 2010;49:243–7.
- [6] Kamyar A, Saidur R, Hasanuzzaman M. Application of computational fluid dynamics (CFD) for nanofluids. *Int J Heat Mass Transfer* 2012;55:15–6. 4104–4115.
- [7] Rana P, Bhargava R. Flow and heat transfer of a nanofluid over a nonlinearly stretching sheet. *Commun Nonlinear Sci Numer Simul* 2012;17:212–26.
- [8] Rashidi MM, Freidoonimehr N, Hosseini A, Anwar Bég O, Hung TK. Homotopy simulation of nanofluid dynamics from a non-linearly stretching isothermal permeable sheet with transpiration of nanofluids over a power law stretching sheet. *Meccanica* 2014;49:469–82.
- [9] Anbuezhian N, Srinivasan K, Chandrasekaran K, Kandasamy R. Thermophoresis and Brownian motion effects on boundary layer flow of nanofluid in presence of thermal stratification due to solar energy. *Appl Math Mech* 2012;33:765–80.
- [10] Alsaedi A, Awais M, Alsaedi A. Effects of heat generation/absorption on stagnation point flow of nanofluid over a surface with convective boundary conditions. *Commun Nonlinear Sci Numer Simul* 2012;17:4210–23.
- [11] Goyal M, Bhargava R. Numerical study of thermodiffusion effects on boundary layer flow. *Microfluid Nanofluid* 2014;17:591–604.
- [12] Van Gorder RA, Sweet E, Vajravelu K. Nano boundary layers over stretching surfaces. *Commun Nonlinear Sci Numer Simul* 2010;15:1494–500.
- [13] Makinde O, Aziz A. Boundary layer flow of a nanofluid past a stretching sheet with a convective boundary condition. *Int J Therm Sci* 2011;50(7):1326–32.
- [14] Akyildiz FT, Bellout H, Vajravelu K, Van Gorder RA. Existence results for third order nonlinear boundary value problems arising in nano boundary layer fluid flows over stretching surfaces. *Nonlinear Anal Ser B: Real World Appl* 2011;12:2919–30.
- [15] Vajravelu K, Prasad KV, Lee J, Lee C, Pop I, Van Gorder RA. Convective heat transfer in the flow of viscous Ag-water and Cu-water nanofluids over a stretching surface. *Int. J. Ther. Sci.* 2011;50:843–51.
- [16] Ahmada A, Asghara S, Alsaedi A. Flow and heat transfer of a nanofluid over a hyperbolically stretching sheet. *Chin Phys B* 2014;23(7):074401.
- [17] Rashidi MM, Freidoonimehr N, Momoniat E, Rostami B. Study of nonlinear MHD tribological squeeze film at generalized magnetic Reynolds numbers using DTM. *PLoS One* 2015;10(8). <http://dx.doi.org/10.1371/journal.pone.0135004>. e0135004.
- [18] Khalili Sadegh, Tamim Hossein, Khalili Arezoo, Rashidi Mohammad Mehdi. Unsteady convective heat and mass transfer in pseudoplastic nanofluid over a stretching wall. *Adv Powder Technol* 2015;26(5):1319–26.
- [19] Ebrahimi-Bajestan Ehsan, Moghadam Mohammad Charjouei, Niazmand Hamid, Daungthongsuk Weerapun, Wongwises Somchai. Experimental and numerical investigation of nanofluids heat transfer characteristics for application in solar heat exchangers. *Int J Heat Mass Transfer* 2016;92:1041–52.
- [20] Mabood F, Shateyi S, Rashidi MM, Momoniat E, Freidoonimehr N. MHD stagnation point flow heat and mass transfer of nanofluids in porous medium with radiation, viscous dissipation and chemical reaction. *Adv. Powder Technol.* 2016;27:742–9.
- [21] Raja M, Vijayan R, Dineshkumar P, Venkatesan M. Review on nanofluids characterization, heat transfer characteristics and applications. *Renewable Sustainable Energy Rev* 2016;64:163–73.
- [22] Lai FC, Kulacki FA. The effect of variable viscosity on convective heat transfer along a vertical surface in a saturated porous medium. *Int J Heat Mass Trans* 1990;33:1028–31.
- [23] Crane LJ. Flow past a stretching plate. *ZAMP* 1970;21:645–7.
- [24] Vajravelu K. Convection heat transfer at a stretching sheet with suction or blowing. *J Math Anal Appl* 1994;188(3):1002–11.
- [25] Ishak A, Nazar R, Pop I. Hydromagnetic flow and heat transfer adjacent to a stretching vertical sheet. *Heat Mass Transfer* 2008;44:921.
- [26] Mukhopadhyay S, Mandal IC, Gorla RSR. Effects of thermal stratification on flow and heat transfer past a porous vertical stretching surface. *J Heat Mass Transfer* 2012;48:915–21.
- [27] Fang Zhang T, Zhong Y. Boundary layer flow over a stretching sheet with variable thickness. *Appl Math Comput* 2012;218:7241–52.
- [28] Lee LL. Boundary layer over a thin needle. *Phys Fluids* 1967;10:822–8.
- [29] Ishak Nazar R, Pop I. Boundary layer flow over a continuously moving thin needle in a parallel free stream. *Chin Phys Lett* 2007;24:2895–7.
- [30] Ahmad S, Arifin NM, Nazar R, Pop I. Mixed convection boundary layer flow along vertical moving thin needles with variable heat flux. *Heat Mass Transfer* 2008;44:473–9.
- [31] Khader MM, Megahed AM. Boundary layer flow due to a stretching sheet with a variable thickness and slip velocity. *J Appl Mech Technol Phy* 2015;6:241–7.
- [32] Prasad KV, Vajravelu K, Vaidya Hanumesh. Hall effect on MHD flow and heat transfer over a stretching sheet with variable thickness. *Int. J. Comput. Methods Eng. Sci. Mech.* 2016. <http://dx.doi.org/10.1080/15502287.2016.1209795>.
- [33] Liao S. Beyond perturbation: introduction to homotopy analysis method. London: Chapman & Hall/CRC Press; 2003.
- [34] Fan T, You X. Optimal homotopy analysis method for nonlinear differential equations in the boundary layer. *Numer Algor* 2013;62(2):337–54.
- [35] Liao S. A new branch of solutions of boundary-layer flows over a permeable stretching plate. *Int J Non-Linear Mech* 2007;42(6):819–30.